Polarization transfer measurements for the $^{13}C(\vec{p},\vec{n})^{13}N$ reaction at 197 MeV and empirical isovector spin-longitudinal response for the $(1/2)^-_{g.s.} \rightarrow (1/2)^+_1$ transition

X. Wang, J. Rapaport, M. Palarczyk,* C. Hautala, and X. Yang
Department of Physics and Astronomy, Ohio University, Athens, Ohio 45701

D. L. Prout,† B. Anderson, A. R. Baldwin, J. Olmsted, J. W. Watson, and W.-M Zhang
Department of Physics, Kent State University, Kent, Ohio 44242

I. Van Heerden,‡ and E. J. Stephenson
Indiana University Cyclotron Facility, Bloomington, Indiana 47405

R. Howes and S. Parks
Department of Physics, Ball State University, Muncie, Indiana 47306

E. Sugarbaker
Department of Physics, The Ohio State University, Columbus, Ohio 43210

B. A. Brown
Department of Physics and Astronomy and National Superconducting Cyclotron Laboratory, Michigan State University, East Lansing, Michigan 48824

F. Sammarruca
Department of Physics, University of Idaho, Moscow, Idaho 83843
(Received 1 March 2002; published 17 July 2002)

We present differential cross sections and complete sets of polarization-transfer coefficients, D_{ij}, obtained in the $^{13}C(\vec{p},\vec{n})^{13}N$ reaction studied at 197 MeV incident proton energy and laboratory angles between 0° and 33°. These complete sets of polarization observables are used to obtain spin-longitudinal and spin-transverse components for transitions to the ground state, to the first, and to the unresolved second and third excited states in ^{13}N at 2.36 MeV and (3.50+3.55) MeV, respectively. The results are used to obtain the two ΔJ^π contributions for the ground and first excited state transitions and are compared with corresponding distorted-wave impulse approximation (DWIA) calculations. In particular, empirical angular distribution values for the unique spin-longitudinal $\Delta J = 0^-$ transition to the first excited state in ^{13}N are obtained and compared with DWIA calculations.

DOI: 10.1103/PhysRevC.66.014606 PACS number(s): 25.40.Kv, 24.70.+s

I. INTRODUCTION

The intermediate energy high-intensity polarized proton beams and the time-of-flight neutron polarimeters available at the Indiana University Cyclotron Facility (IUCF) have allowed the measurement of complete sets of polarization-transfer coefficients in $(\vec{p},\vec{n})$ reactions. With this data, it is possible to differentiate between natural and unnatural parity contributions to differential cross sections. This is particularly useful in cases where the target ground state (g.s.) angular momentum is half integral and the contributions add incoherently to the differential cross sections.

Previous experimental studies of the (p,n) reaction at intermediate energies have examined and provided much information on isovector modes of excitation in nuclei. The reactions studied include spin-monopole (Gamow-Teller), spin-dipole, and spin-quadrupole transitions [1,2]. The $\Delta L = 1$, $\Delta S = 1$, $\Delta J = 0^-$ spin-dipole transition (known in β decay as a unique first forbidden decay) holds a special place among these transitions despite its low strength because it carries the pion quantum numbers and corresponds to a pure spin-longitudinal transition.

In general, the excitation of the spin-dipole resonance via the (p,n) reaction includes $\Delta J^\pi = 0^-$, 1^-, and 2^- components. These components overlap in the giant spin-dipole broad resonance. They are mixed with the excitation of the giant dipole resonance, $\Delta J^\pi = 1^-$, and cannot easily be disentangled. Centroid locations of the spin-dipole resonances have been studied in charge exchange reactions [3] and compared with random-phase approximation calculations. In the energy range from 40 to 200 MeV, the excitation of the spin-dipole resonance increases with the incident energy of the probe [1]. A recent experiment studied the splitting of the

*Permanent address: Henryk Niewodniczański Institute of Nuclear Physics, 31-342 Kraków, Poland.

†Permanent address: DOE Remote Sensing Lab., Las Vegas, Nevada 89115.

‡Permanent address: University of the Western Cape, South Africa.

dipole and spin-dipole resonances in charge exchange reactions using the fact that their relative excitation is expected to change in this energy range [4].

In a previous paper [5], we presented zero-degree differential cross sections and complete sets of polarization-transfer coefficients for the $^{13}C(\vec{p},\vec{n})^{13}N$ reaction at 197 MeV incident proton energy. We used a complete set of D_{ij} values for the g.s. transition to separate the Fermi (F) and Gamow-Teller (GT) contributions to the cross section and to deduce the GT transition strengths. In the present paper, we extend the angular range up to $\theta_{lab}=33°$. For the first time, we use the complete set of D_{ij} coefficients to obtain the unnatural parity (GT) and natural parity (Fermi) contributions to the g.s. differential cross section. These measurements can also separate the spin-longitudinal, $\Delta J=0^-$, and spin-transverse, $\Delta J=1^-$, contributions to the $J^\pi=(1/2)^+$ first excited state in ^{13}N (2.36 MeV).

Our present understanding is that the *NN* interaction at intermediate energies is mediated by meson exchange and that the long range behavior of the interaction is dominated by one pion exchange. According to model calculations [6,7], the effects of meson exchange are reflected in the momentum transfer dependence of the spin-longitudinal nuclear response which is inaccessible to electromagnetic probes. Thus, it is of considerable interest to empirically obtain the nuclear response to a probe that induces a nuclear transition with no change in the total angular momentum but with a parity change, which is a $\Delta J^\pi=0^-$ transition. This type of transition carries the quantum numbers of the pion and corresponds to a pure spin-longitudinal transition. The real part of the spin-longitudinal interaction crosses zero near $q\approx 0.7$ fm^{-1}. The precise location of the zero crossing is a sensitive test of whether the nuclear medium contains extra attraction (zero crossing at lower q) or repulsion from some mechanism such as ρ-meson mass rescaling [8].

Pionic-like nuclear excitations are preferentially studied in nuclear $\Delta J^\pi=0^+\rightarrow\Delta J^\pi=0^-$ transitions, but there are only a few isovector transitions of this type experimentally accessible. One of these is the $^{16}O(p,n)^{16}F$(g.s.) transition which is only 193 keV below the 1_1^- state and 424 keV below the usually strongly excited 2_1^- state [9] in ^{16}F. This reaction has been studied at $E_p=35$ MeV [10] and at $E_p=79$ MeV [11]. The experimental energy resolution needed to clearly separate the three spin-dipole states was achieved by Orihara *et al.* [10] at $E_p=35$ MeV. However, at this low energy, the interpretation of the results is less transparent than at intermediate energies (120 MeV–300 MeV) because of the relative importance of distortions, exchange processes, ambiguities in the effective nuclear interaction, the contributions of higher order effects, etc. The experimental results at $E_p=79$ MeV for the differential cross section to the ^{16}F(g.s.) transition reported by Madey *et al.* [11] compare reasonably well with distorted-wave impulse approximation (DWIA) calculations in the momentum transfer range $0.21\leqslant q\leqslant 2.0$ fm^{-1}. However the calculations significantly overestimate the measured differential cross sections at larger momentum transfer. These results are in sharp disagreement with those reported at $E_p=35$ MeV [10]. At lower incident energy, the experimental differential cross sections at large momentum transfer are much larger than the predictions of impulse approximation (IA) calculations. The authors interpret this disagreement as a possible signature of meson-exchange currents. However, it is known that IA calculations are more reliable in describing inelastic scattering data at incident energies above 100 MeV [12], a concern that applies to both sets of data described above.

Proton inelastic scattering data for transitions leading to $J^\pi=0^-$ states in ^{16}O have been reported by Hosono *et al.* [13] at $E_p=65$ MeV and by Sawafta *et al.* [14] at 200 MeV. These authors have studied the isoscalar 0^- transition to the excited state at $E_x=10.957$ MeV and the isovector 0^- transition to the excited state at $E_x=12.796$ MeV. Their experimental results at 65 MeV for the isovector $T=1$ analog-state transition are in fair agreement with DWIA calculations. Preliminary results for the same transition at 200 MeV by Stephenson *et al.* [15] show good agreement with DWIA calculations for the differential cross section although the analyzing powers are not described as well.

Other charge exchange (p,n) transitions, experimentally more attractive and containing information about $0^+\rightarrow 0^-$ transitions, are the $(1/2)^-\rightarrow(1/2)^+$ transitions. These transitions are mediated by incoherent contributions of $\Delta J^\pi=1^-$ and $\Delta J^\pi=0^-$ transfers. Examples of these are the $^{13}C(p,n)^{13}N$ (2.36 MeV) and the $^{15}N(p,n)^{15}O$ (7.56 MeV) transitions. Orihara *et al.* [16] have studied these transitions at $E_p=35$ MeV with results similar to the studies at the same incident energy of the (p,n) reaction on an ^{16}O target [10].

In this paper, we present differential cross section data and a complete set of polarization-transfer observables for the $^{13}C(\vec{p},\vec{n})^{13}N$ reaction obtained at $E_p=197$ MeV and at a range of angles between 0° and 33°. The experiment was performed using the IUCF facilities. The analysis of the data is focused on the g.s. and first excited state transition in ^{13}N, all of which have different incoherent admixtures of multipolarities. In particular, the $(1/2)^-\rightarrow(1/2)^-$ g.s. transition is mediated via Fermi, $\Delta J^\pi=0^+$, and Gamow-Teller, $\Delta J^\pi=1^+$, transitions. The $(1/2)^-\rightarrow(1/2)^+$ transition to the first excited state at $E_x=2.36$ MeV is mediated via the unique spin-dipole $\Delta J^\pi=0^-$ and dipole/spin-dipole $\Delta J^\pi=1^-$ transitions. We also present data to the unresolved second and third excited states in ^{13}N at 3.50 and 3.55 MeV. The main contribution to the measured differential cross section, especially for momentum transfers below 1.0 fm^{-1}, comes from the $(1/2)^-\rightarrow(3/2)^-$ 3.50 MeV transition. This transition is mediated via $\Delta J^\pi=1^+$, Gamow-Teller, and quadrupole/spin-quadrupole $\Delta J^\pi=2^+$ contributions.

The complete set of polarization-transfer observables allows a unique separation of natural and unnatural components and a separation of the unique spin-dipole transition.

II. EXPERIMENTAL METHODS AND DATA ANALYSIS

The experiment was performed at the IUCF using the beam swinger, the Indiana Neutron Polarization (INPOL) facility, and the Kent State University (KSU) "2π" neutron polarimeter. Polarized protons with an energy of 197 MeV

were focused on a self-supported, $(89\pm4)\%$ isotopically enriched ^{13}C target with a total thickness of 146 mg/cm^2. The enrichment of the target was measured with an inductively coupled plasma mass spectrometer. Detailed descriptions of the INPOL facility and the neutron polarimeter systems can be found in Refs. [17,18]. Only the details of the experimental setup relevant to the present experiment are described here.

A. Polarized proton beam

The high intensity polarized ion source (HIPIOS) [19] was used to provide 70% polarized proton beams with intensities up to 380 nA in subnanosecond pulses separated by about 170 ns. The beam polarization was cycled between ''normal'' and ''reverse'' at 30 sec intervals. Superconducting solenoids located in the proton beam line were used to precess the proton spin polarization so as to have on target any one of the three spin states, normal $(\hat{N})$, sideways $(\hat{S})$, or longitudinal $(\hat{L})$. The settings of the solenoids take into account the precession caused by the swinger magnets. The value of the proton beam polarization was continuously measured with beam line polarimeters located immediately after the superconducting solenoids [20].

B. Neutron beam lines

Magnets located after the target were used to precess the neutron spin to a desirable orientation for measurement of the three components of its spin vector. In cases where the incident proton spin was in a normal orientation, superconducting solenoids were used to rotate the neutron spin both $+90°$ and $-90°$ about the momentum axis during separate series of runs to correct for possible geometrical asymmetries in the polarimeters. In another series of runs, dipole magnets were used to precess the longitudinal component of the neutron spin to a direction normal to the neutron's momentum so that this spin component was measurable in the neutron polarimeters.

C. INPOL polarimeter

A large volume neutron polarimeter [17] located in the $0°$ neutron beam line was used to measure the polarization of neutrons emitted in the $^{13}\mathrm{C}(\vec{p},\vec{n})^{13}\mathrm{N}$ reaction. The polarimeter consists of four parallel detector ''planes'' oriented perpendicular to the incident neutron flux. Each 1 m^2 ''plane'' consists of ten scintillators each 10 cm high, 10 cm thick, and 1 m long. The first three of these planes are stainless steel tanks filled with Bicron BC-517S liquid scintillator chosen for its high hydrogen content (H:C = 1.7). The fourth plane is made of BC-408 plastic scintillator and also consists of ten separate detectors. The front two scintillator planes are used as neutron polarization analyzers. Time, position, and pulse-height information from the front and back planes is used to select np scattering kinematics and to provide analyzing power to measure the neutron polarization. Thin plastic scintillators in front of these planes are used to tag charged particles. During these experiments, intrinsic time resolution of about 300 ps [full width at half maximum (FWHM)] and position resolution of about 4.5 cm (FWHM) were usually obtained. The neutron flight path to the first plane of these detectors was measured to be 159 m.

D. KSU 2π polarimeter

The KSU 2π polarimeter [18] consists of four, 10-cm-high, 10-cm-wide, and 50-cm-long BC-404 plastic scintillators that are used as neutron scatterers or analyzers. The scintillators are situated along the long axis along the neutron's direction of motion. Displaced 160-cm downstream from the center of the front four scintillators is an azimuthally symmetric ''ring'' of 12 large BC-400 plastic scintillation detectors of dimensions 10 cm high by 25 cm wide and 1 m long. The ring has a diameter of 116 cm. The scattering angle between the center of the analyzer detectors and the center of any of the ring detectors is $20°$.

Neutrons scattered from the analyzers are detected in this complete azimuthal coverage. All 16 detectors are mean timed using fast photomultiplier tubes on each end of the scintillators. Time, position, and pulse height information from the central and cylindrical detectors was used to define np scattering kinematics for forward angle neutrons. An intrinsic time resolution of about 120 ps (FWHM) and a position resolution of about 1.7 cm (FWHM) were obtained. Taking the ^{13}C target thickness into consideration, we set the neutron flight path to the analyzer to 49.6 m to achieve the needed energy resolution for this experiment.

E. Polarimeter cross calibrations

In a separate experiment, polarization data were taken for the $^6\mathrm{Li}(\vec{p},\vec{n})^6\mathrm{Be}$ reaction at $24°$ with both polarimeters [21]. The comparison of cross section and polarization data over the large energy range of the quasielastic peak produced consistent results that generally agreed to better than 10%.

Neutron energies were measured by the time of flight from the target to the front detector with an overall energy resolution that was about 600 keV (FWHM) mainly due to the ^{13}C target thickness. For INPOL, absolute differential cross sections were obtained using the method described in Ref. [17]. Briefly, the product of the neutron detector efficiency for double scattering and the neutron absorption in air and other materials over the 159-m neutron flight path was measured in previous experiments. These used the $^7\mathrm{Li}(\vec{p},\vec{n})^7\mathrm{Be}$ reaction in which the conditions were identical to those of the current experimental conditions. The $0°$-differential cross section for this reaction is well known from activation measurements in the energy range between 80–800 MeV [22]. The neutron energy dependence for these normalization factors had been obtained previously [17]. For the KSU 2π polarimeter, absolute differential cross sections were determined by comparing cross section data obtained at $24°$ for the $^7\mathrm{Li}(\vec{p},\vec{n})^7\mathrm{Be}$ reaction and for the $^{12}\mathrm{C}(\vec{p},\vec{n})^{12}\mathrm{N}$ reaction with earlier absolute cross section measurements of these reactions [23].

III. DATA ANALYSIS

The data taken during the experiment were stored on magnetic tapes which were processed off-line. Fitting of the

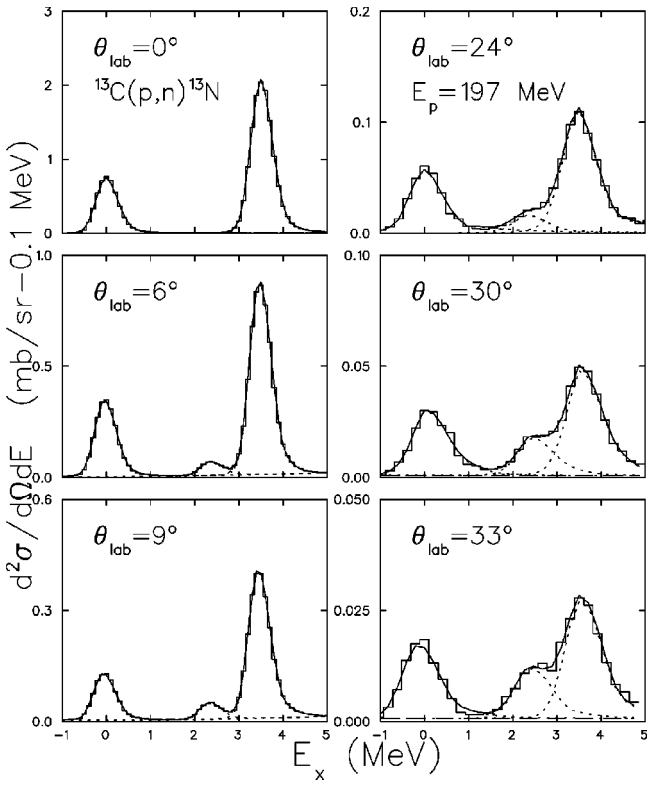

FIG. 1. Excitation energy spectra for the $^{13}C(p,n)^{13}N$ reaction obtained at $E_p=197$ MeV at the indicated scattering angles. Only data up to 5 MeV excitation energy are presented. The dashed curves represent individual peak fits, while the solid curves indicate the sum peak fit including the background shown as dotted curves.

spectra was performed with the line-shape fitting code ALLFIT [24] as described in Ref. [5].

To start the fitting procedure, the g.s. transition, which corresponds to a well isolated peak was fitted to obtain the best parameters for the corresponding line shape. These parameters were then used to fit the spectra up to 5 MeV of excitation including the g.s., the first excited state at 2.36 MeV, and the peak representing the unresolved excited states at 3.50 and 3.55 MeV. Because of the overall energy resolution, 600 keV (FWHM), it was not feasible to separate these two states and were considered in the fitting analysis as a single peak. A total of nine spectra were analyzed at each scattering angle for each type of polarized proton beam: four spectra corresponding to the four sectors into which the neutron polarimeter was divided [17](up, down, left, and right) for a polarized proton beam, and four corresponding to the sectors for a proton beam with reversed polarization. An additional spectrum representing the summation of the eight spectra was also considered. All nine spectra were fitted with the same set of line-shape and background functions. Typically, $\chi^2/\nu \approx 2$ were obtained. In Fig. 1 we show fitted results for the sum spectra up to 5 MeV of excitation in ^{13}N obtained at all the angles studied in this paper. The dotted lines represent the results of individual peak fittings while the solid curves represent the sum of these contributions. At some angles, a background represented by dot-dashed curves is also shown. The background in this excitation energy range is minimal as may be judged from the zero-degree spectrum shown in Ref. [5].

IV. DATA REDUCTION

The polarization-transfer coefficients, $D_{ij}(i=S',N',L',j=S,N,L)$, relate the outgoing neutron (i) polarization to the incident proton (j) polarization according to [25]

$$\begin{pmatrix} p'_{S'} \\ p'_{N'} \\ p'_{L'} \end{pmatrix} = \left[\begin{pmatrix} D_{S'S} & 0 & D_{S'L} \\ 0 & D_{N'N} & 0 \\ D_{L'S} & 0 & D_{L'L} \end{pmatrix} \begin{pmatrix} p_S \\ p_N \\ p_L \end{pmatrix} + \begin{pmatrix} 0 \\ P \\ 0 \end{pmatrix} \right] \frac{1}{1+p_N A_y}, \quad (1)$$

where $\vec{p}(p_S,p_N,p_L)$ represents the incident proton polarization and $\vec{p}'(p'_{S'},p'_{N'},p'_{L'})$ indicates the outgoing neutron polarization. The directions of the coordinate system are defined in terms of the incident proton momentum $\vec{k}_{lab}$ and the outgoing neutron momentum $\vec{k}'_{lab}$ in the laboratory frame of reference as $\hat{\mathbf{L}}=\hat{\mathbf{k}}_{lab}$, $\hat{\mathbf{L}}'=\hat{\mathbf{k}}'_{lab}$, $\hat{\mathbf{N}}=\hat{\mathbf{N}}'=(\hat{\mathbf{k}}_{lab}\times\hat{\mathbf{k}}'_{lab})/|\hat{\mathbf{k}}_{lab}\times\hat{\mathbf{k}}'_{lab}|$, $\hat{\mathbf{S}}=\hat{\mathbf{N}}\times\hat{\mathbf{L}}$, and $\hat{\mathbf{S}}'=\hat{\mathbf{N}}'\times\hat{\mathbf{L}}'$.

The incident proton beam was tuned so as to have a polarization with a single dominant component on the target. The beam polarization was continuously monitored, and this goal was usually achieved. However, if the beam polarization had components other than the one selected to a level higher than 5%, the beam was stopped and retuned. In the data analysis, these additional small beam polarization components were considered. Values for the analyzing power A_y, the induced polarization P, and the transfer coefficient $D_{N'N}$, were obtained from results with a normally polarized proton beam. The in-plane observables, $D_{S'S}$, $D_{L'S}$ and $D_{L'L}$, $D_{S'L}$, were calculated using results obtained with sideways and longitudinally polarized proton beams, respectively. In what follows, we will use the notation D_{ij} without the primes to denote polarization-transfer coefficients, where i represents the outgoing nucleon and j, the incident nucleon.

V. EXPERIMENTAL RESULTS AND ANALYSIS

All tabulated data have been transmitted to the National Nuclear Data Center at Brookhaven National Lab where they can be retrieved from the CSISRS database at www.nndc.bnl.gov. Only statistical uncertainties in the measured differential cross sections are listed in the tables. To obtain absolute uncertainties, one needs to add in quadrature a 7% error due to uncertainties in target thickness, enrichment of ^{13}C, and neutron polarimeter efficiency.

The angular distributions for the center-of-mass (c.m.) differential cross sections as a function of momentum transfer, q, are presented in Fig. 2. The dashed and dot-dashed curves represent the calculated DWIA contributions from the

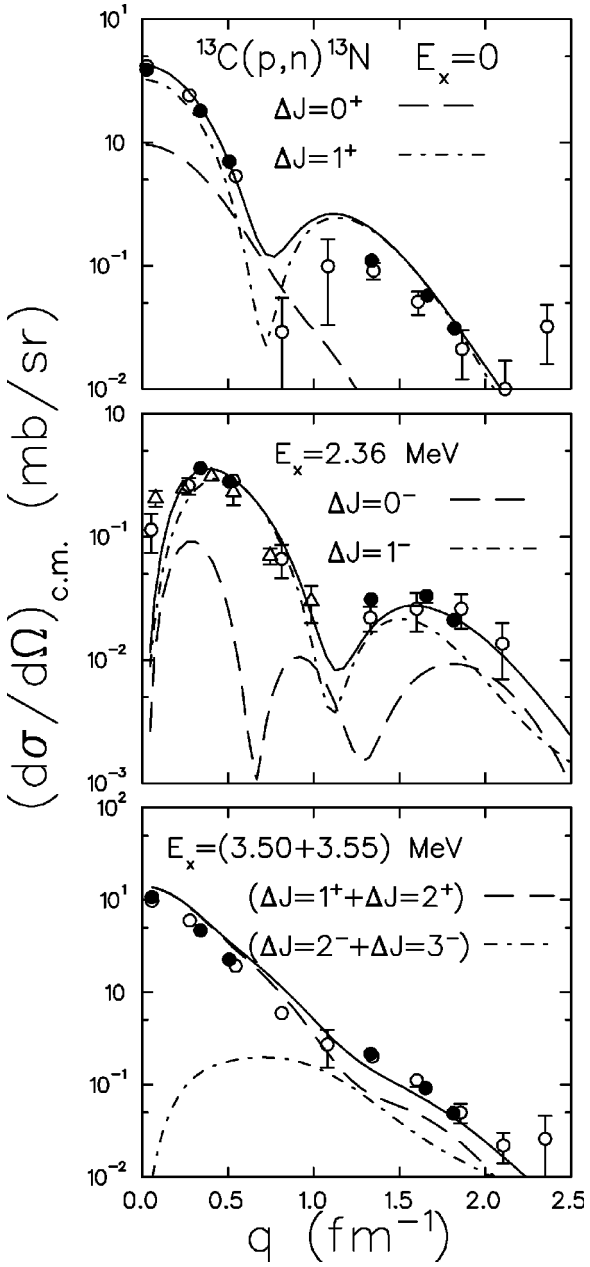

FIG. 2. Differential angular distribution cross sections for the g.s. $[J^\pi=(1/2)^-]$, first excited state $[J^\pi=(1/2)^+]$, and unresolved second $[J^\pi=(3/2)^-]$ and third $[J^\pi=(5/2)^+]$ excited states in ^{13}N measured in the ^{13}C$(\vec{p},\vec{n})$ reaction at $E_p=197$ MeV. The solid data points correspond to this experiment. The open circle symbols and open triangle symbols correspond to data taken for these transitions at $E_p=160$ and $E_p=186$ MeV. The curves are DWIA calculations for the indicated spin-transfer transitions. The solid curves represent the incoherent sum of the transitions.

two types of ΔJ multipolarities in each transition. The solid curves represent the incoherent sum of these components. Differential cross section data previously obtained for these transitions at $E_p=160$ and 186 MeV are also included in the figures with open circle symbols and open triangle symbols, respectively [26].

The bottom panel in Fig. 2 represents differential cross

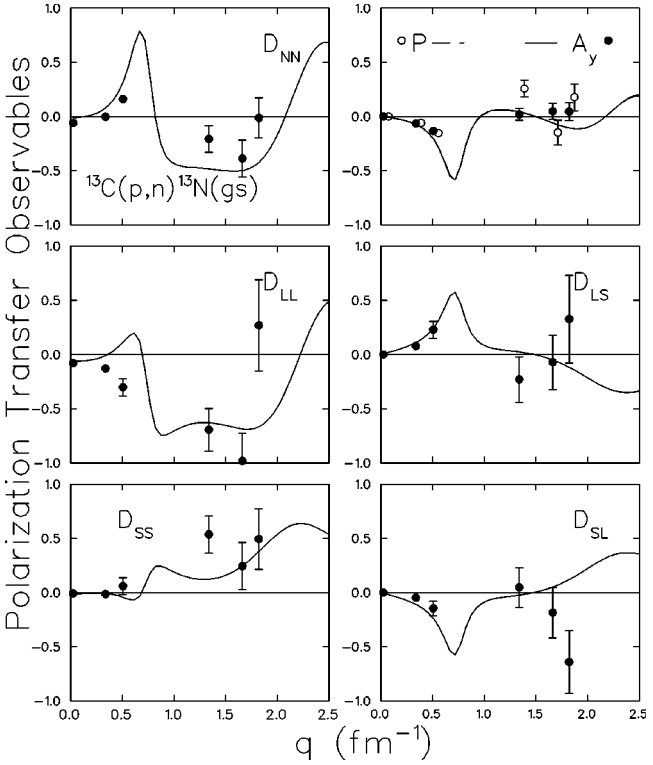

FIG. 3. Differential angular distribution for polarization-transfer coefficients, analyzing power, and induced polarization for the g.s. transition in the ^{13}C$(\vec{p},\vec{n})$ reaction at $E_p=197$ MeV. The curves are DWIA calculations. See text.

section data for the unresolved transitions to the $J^\pi=(3/2)^-$, 3.50 MeV state and to the $J^\pi=(5/2)^+$, 3.55 MeV state in ^{13}N. For momentum-transfer values up to about 1 fm^{-1} the experimental points are well reproduced by the shape of the calculated $\Delta J=(1^++2^+)$ transitions to the 3.50 MeV state represented as dashed lines in the figure. We have done calculations for $\Delta J=(2^-+3^-)$ transitions that excite the $J^\pi=(5/2)^+$ state indicated as dot-dashed lines in the figure. The predicted maximum differential cross section occurs at about 0.7 fm-1.

In Figs. 3–5, we present D_{ij}, A_y, and P values for the g.s., first excited state, and unresolved second and third excited state transitions studied in this work. The curves are DWIA calculations to be described in the following section. The uncertainties in the back angle values are larger than those in the forward angles because the differential cross sections are about an order of magnitude smaller. In the top right frame of each figure, values for A_y and P are shown. The latter observables have been offset by a momentum transfer $q=0.05$ fm^{-1} so that they can be visualized clearly. The dot-dashed DWIA curves shown in Fig. 5 correspond to the transition to the $J^\pi=(3/2)^-$, 3.50 MeV state. The solid lines correspond to DWIA calculations that include contributions for the transitions to the 3.55 MeV state.

As indicated earlier, the enrichment of ^{13}C in the target was $(89\pm4)\%$. Thus the target contained 11% ^{12}C. Spectra obtained with a ^{nat}C target, 99% ^{12}C, were properly subtracted from spectra recorded with the enriched target. The

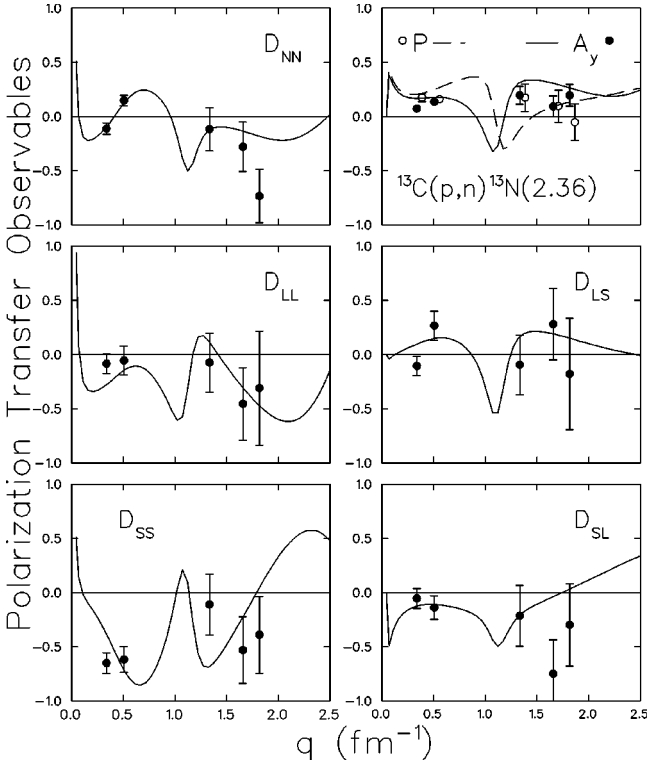

FIG. 4. Same as in Fig. 3 but for the transition to the first excited state, 2.36 MeV, in ^{13}N.

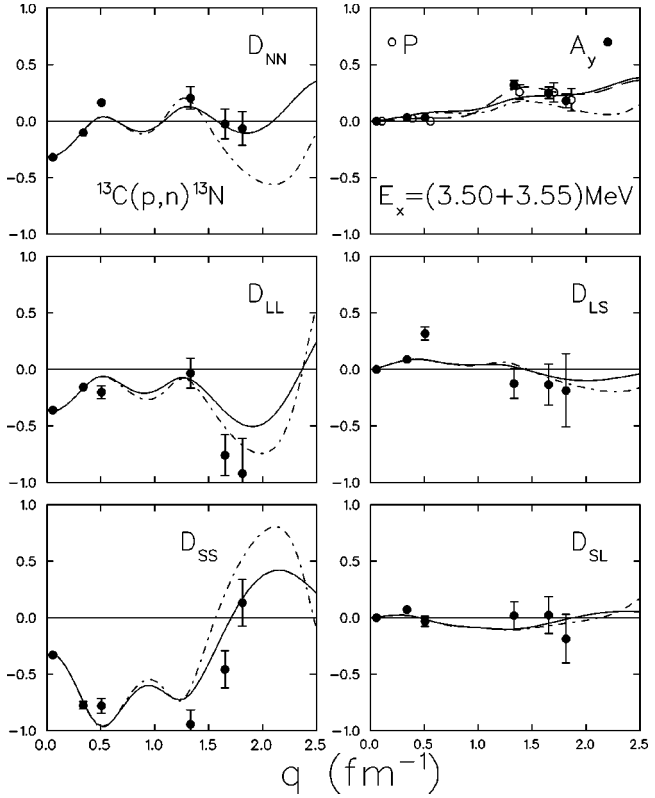

FIG. 5. Same as in Fig. 3 but for transitions to the unresolved excited states at 3.50 and 3.55 MeV in ^{13}N. The dotted lines represent DWIA calculations for the $J^{\pi}=(3/2)^{-}$, 3.50 MeV state. The solid lines include estimated contributions from DWIA calculations for the $J^{\pi}=(5/2)^{+}$, 3.55 MeV state.

main contribution of the ^{12}C is due to its g.s. transition that has the same Q value as the ^{13}C$(p,n)^{13}$N transition to the 15.1 MeV excited state. Therefore it does not affect the results presented in this study which extend only up to 5.0 MeV of excitation in ^{13}N.

A. Distorted-wave calculations

Theoretical differential cross sections and D_{ij} coefficients were obtained with microscopic DWIA calculations. These were done using the computer code DW81 [27] in which the knock-out exchange amplitudes are treated exactly. The basic ingredients needed in this code are briefly indicated below.

The free nucleon-nucleon interaction parametrized by Franey and Love [28] was used as the interaction between the incident and struck nucleons. The set of interaction parameters reported at $E_p=210$ MeV were used in the DWIA calculations. A more recent parametrization developed by Love [29] produced almost identical results.

The shell-model code OXBASH [30] was used to calculate the one body density matrix elements (OBDME). Only transitions characterized as $0\hbar\omega\, p\rightarrow p$ and $1\hbar\omega\, p\rightarrow p$ were included for the positive and negative parity transitions. The OBDME values were obtained using the interaction derived by Warburton and Brown using least-square fits to 51 $1p$-shell and 165 cross-shell binding energies [31]. Either harmonic oscillator (HO) or Woods-Saxon potential (WS) wave functions were assumed for the single particle states. In DWIA calculations for light nuclei, the center-of-mass corrections are important. These corrections were made as described by Brady *et al.* in the Appendix of Ref. [32]. A reduced HO size parameter, $b_o=1.87$ fm, was used to calculate the single particle states. This reduced HO size parameter is based on an analysis of the transverse form factor obtained from (e,e') scattering on ^{13}C [33]. The Woods-Saxon geometry parameters were adjusted until a calculation of the transverse form factor in (e,e') inelastic scattering reproduced the measurements. The binding energies were chosen to represent the energy needed to separate a proton or a neutron leaving behind the lowest state with the required spin and parity.

The shape of the calculated differential cross sections was not greatly affected by the choice of either the HO or the WS potential in the description of the single particle states. However, using the WS potential made a significant improvement in the comparison of the calculations to the data for the transition to the 2.36 MeV state especially in the momentum transfer region between 1.0 and 2.0 fm^{-1}. It did not greatly affect the DWIA results for the other two transitions. As may be seen in Fig. 2, the DWIA results obtained with the WS potential agree well with empirical values. The differential cross sections obtained with an HO potential were about two to three times lower than the empirical values at larger momentum transfers.

Distorted waves for incident and outgoing nucleons were calculated using optical model potential (OMP) parameters obtained from proton elastic scattering data for ^{12}C [34]. The energy dependence of OMP parameters was taken into ac-

count as suggested in Ref. [34]. The isospin effect as well as the Coulomb correction potential were applied to the OMP parameters for describing the unpaired nucleon [35].

The curves shown in Figs. 2–5 correspond to these calculations. In Fig. 2 (top frame) for the g.s. transition, no normalization was used for the Fermi contribution while a normalization factor $N=0.2/0.1746$ was used for the GT transition. This factor corresponds to the ratio between the empirical g.s. GT strength, 0.2 GT units, and the shell-model-calculated value, 0.1746 GT units [5]. For the 2.36 MeV transition (middle-frame), an overall normalization factor of 0.28 was used to match the calculated and empirical differential cross sections. This value is lower than the value 0.5, which we reported previously in Ref. [5] and which was obtained with the use of an HO potential instead of a WS potential in the calculation of wave functions for the single particle states. Madey *et al.* [11] used a normalization of 0.35 in their DWIA representation of the empirical data for the $^{16}O(p,n)^{16}F(1^-,0.19\ \text{MeV})$ transition, while Hosono [13] used a normalization of 0.48 in the distorted-wave Born approximation calculation for the $^{16}O(p,p')^{16}O(0^-,12.8\ \text{MeV},T=1)$ transition. In a recent paper, Auerbach and Brown [36] describe weak interaction rates in ^{12}C, ^{14}N, and ^{16}O and use the same model space as in this work. They find that the best overall agreement with experiment for the total strength is obtained with a quenching of 0.64. The present normalization for the dipole transition, a small fraction of the total strength, is somewhat lower than, but within the range of, other similar experiments. The GT component in the transition to the 3.50 MeV state (bottom frame) was normalized by the ratio between empirical GT strength, 1.06 GT units, and the shell-model-calculated value, 1.34 GT units. A normalization of 1.0 was used for the quadrupole component. The calculated differential cross sections for the transitions to the 3.55 MeV state ($\Delta J=2^-$ and $\Delta J=3^-$), were normalized by 0.1 and added to the cross sections for the 3.50 MeV state. The result is shown as a full line in Fig. 2.

B. Polarization observables

We follow the procedure outlined by Ichimura and Kawahigashi [37], which uses relativistic transformations of observables to define four c.m. frame polarization observables D_k in terms of the laboratory-frame polarization-transfer coefficients D_{ij}. These polarization observables are given by

$$D_o=(1/4)[1+D_{N'N}+(D_{S'S}+D_{L'L})\cos(\alpha_1) -(D_{S'L}-D_{L'S})\sin(\alpha_1)], \tag{2}$$

$$D_n=(1/4)[1+D_{N'N}-(D_{S'S}+D_{L'L})\cos(\alpha_1) +(D_{S'L}-D_{L'S})\sin(\alpha_1)], \tag{3}$$

$$D_q=(1/4)[1-D_{N'N}+(D_{S'S}-D_{L'L})\cos(\alpha_2) -(D_{S'L}+D_{L'S})\sin(\alpha_2)], \tag{4}$$

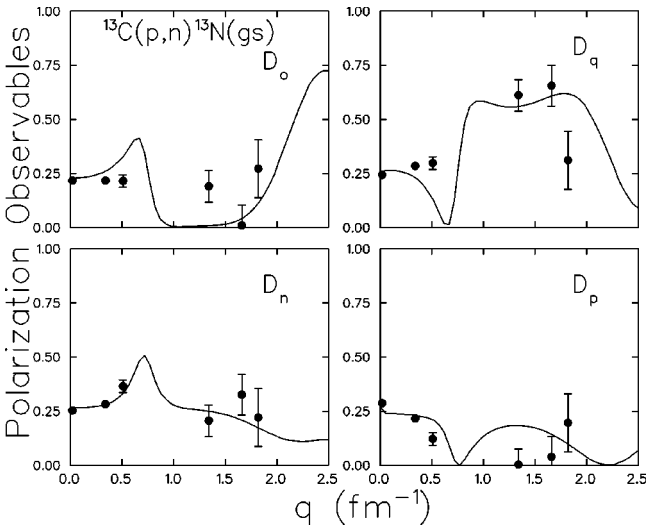

FIG. 6. Polarization observables for the reaction $^{13}C(\vec{p},\vec{n})^{13}N(g.s.)$ at $E_p=197$ MeV as a function of momentum transfer, q, compared to DWIA results (solid lines). See text.

$$D_p=(1/4)[1-D_{N'N}-(D_{S'S}-D_{L'L})\cos(\alpha_2) +(D_{S'L}+D_{L'S})\sin(\alpha_2)], \tag{5}$$

with the constraint

$$D_o+D_n+D_q+D_p=1. \tag{6}$$

These observables follow from the original definitions of Bleszynski, Bleszynski, and Whitten [38] and are spin independent (D_o), spin longitudinal (D_q), and spin transverse (D_n and D_p).

The laboratory-frame coordinates (S,N,L) and (S',N',L') were defined in Sec. IV. The corresponding c.m. coordinates (q,n,p) are defined as $\mathbf{q}=(\mathbf{k}_f-\mathbf{k}_i)/(|\mathbf{k}_f-\mathbf{k}_i|)$, $\mathbf{n}=(\mathbf{k}_i\times\mathbf{k}_f)/(|\mathbf{k}_i\times\mathbf{k}_f|)$, and $\mathbf{p}=\mathbf{q}\times\mathbf{n}$, where k_i and k_f are the initial and final projectile momenta in the *NA* c.m. frame. The angles α_1 and α_2 are defined by

$$\alpha_1=\theta_{\text{c.m.}}-\alpha_0, \tag{7}$$

$$\alpha_2=2\,\theta_p-\theta_{\text{c.m.}}+\alpha_0, \tag{8}$$

where

$$\cos(\alpha_0)=\cos(\theta_{\text{c.m.}})\cos(\theta_{lab})+\gamma\sin(\theta_{\text{c.m.}})\sin(\theta_{lab}). \tag{9}$$

The angle α_0 is related to the relativistic angle Ω used by Ichimura and Kawahigashi [37] by $\alpha_0=\theta_{\text{c.m.}}-\theta_{lab}-\Omega$. The angle θ_p represents the angle between the incident beam direction and the vector $\mathbf{p}$ defined above.

The calculated c.m. polarization observables, D_k, are plotted as a function of momentum transfer, q, in Figs. 6–8 for the transitions to the g.s., the first excited state, and the second excited state in ^{13}N, respectively.

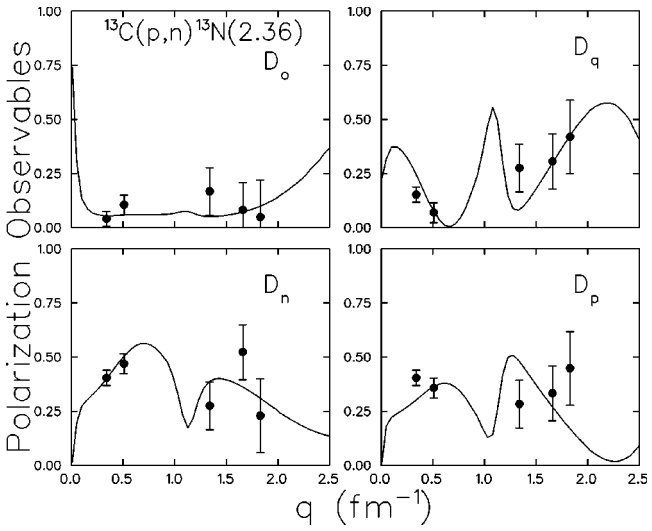

FIG. 7. Same as in Fig. 6 but for the transition to the 2.36 MeV excited state in ^{13}N.

The significance of the c.m. observables, D_k, becomes apparent in their application to free *NN* scattering [25]. In its standard form [39], the c.m. *NN* charge-exchange scattering amplitude is expressed as

$$M(q)=A+C(\sigma_{0n}+\sigma_{1n})+B\sigma_{0n}\sigma_{1n}+E\sigma_{0q}\sigma_{1q}+F\sigma_{0p}\sigma_{1p}, \quad (10)$$

where σ_0 and σ_1 are the Pauli spin matrices for the projectile and target nucleons projected onto the *NN* c.m. coordinate axes, (q,n,p). In this case, the *NN* c.m. partial cross sections [37]

$$I_o^{NN}=I^{NN}D_o^{NN}=|A|^2+|C|^2, \quad (11)$$

$$I_n^{NN}=I^{NN}D_n^{NN}=|B|^2+|C|^2, \quad (12)$$

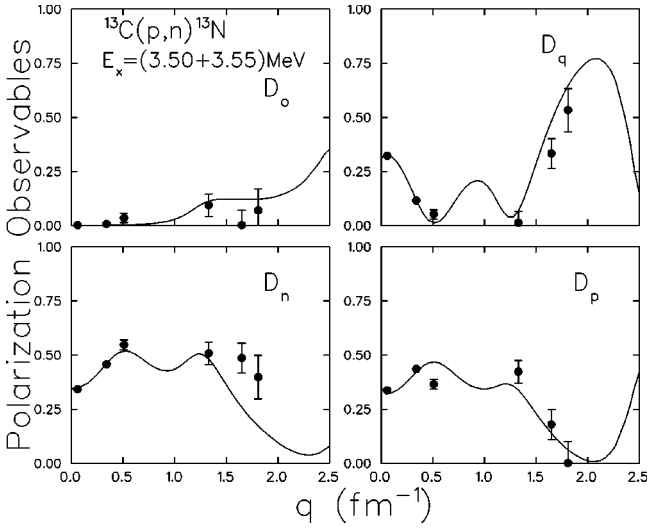

FIG. 8. Same as in Fig. 6 but for transitions to the unresolved excited states at 3.50 and 3.55 MeV in ^{13}N. The DWIA calculations are just for the 3.50 MeV transition.

$$I_q^{NN}=I^{NN}D_q^{NN}=|E|^2, \quad (13)$$

$$I_p^{NN}=I^{NN}D_p^{NN}=|F|^2, \quad (14)$$

select simple combinations of amplitudes. At zero degree the subscript "*o*" represents the spin independent component. At other angles it includes the spin-orbit component. The subscript "*q*" represents the spin-longitudinal component, and "*n*" and "*p*" the two spin-transverse components. The sum of the polarization components, $\Sigma_k D_k^{NN}=1$.

Here we see that $I^{NN}D_q^{NN}$ and $I^{NN}D_p^{NN}$ depend only on the spin-longitudinal and spin-transverse parts of the *NN* c.m. amplitudes, respectively. In a plane wave impulse approximation for an arbitrary target, i.e., a nucleon-nucleus (*NA*) case, ID_q and ID_p are expected to represent the spin-longitudinal and spin-transverse responses exclusively [37]. In this general case, this can be written

$$I_q=ID_q=|E|^2\chi_L^2, \quad I_p=ID_p=|F|^2\chi_T^2, \quad (15)$$

where χ_L and χ_T are the spin-longitudinal and spin-transverse form factors. The *NA* differential cross section, *I*, can be represented as a sum of terms [25],

$$I=ID_o+ID_q+ID_n+ID_p, \quad (16)$$

where the D_k are the polarization components defined in Eqs. (2)–(6) [38].

In Fig. 9, we show the differential angular distribution cross sections for the g.s. and first excited state in ^{13}N. For the g.s. transition (top frame), the filled triangle symbols represent ID_o, the non-spin-transfer or Fermi component. The short dashed curve corresponds to the DWIA cross section. In the bottom-panel, the filled diamond symbols represent ID_q, the spin-longitudinal partial cross section. In this case, it represents the $\Delta J^\pi=0^-$ component of this transition.

VI. RESULTS AND DISCUSSION

One of the objectives of this paper has been to obtain the the empirical partial cross sections for the Fermi component of the angular distribution of the differential cross sections for the g.s. transition and for the spin-dipole $\Delta J^\pi=0^-$ transition to the 2.36 MeV state in ^{13}N. This has been achieved with the measured spin-transfer coefficients for these transitions. However, we can learn more by comparing our results to the predictions of state-of-the-art theoretical models. In previous sections, we have described DWIA calculations using empirical optical model potentials and parametrizations of the free *NN* interaction. The calculations are generally in agreement with the experimental results. However, a self-consistent calculation that describes spin-transfer transitions fairly well [40] has recently been obtained using the density-dependent DBHF (Dirac-Brueckner Hartree-Fock) interaction of Sammarruca and co-workers [40,41]. We compare results of these calculations to our data.

The starting point of this calculation is a realistic free-space *NN* interaction which reproduces well *NN* scattering

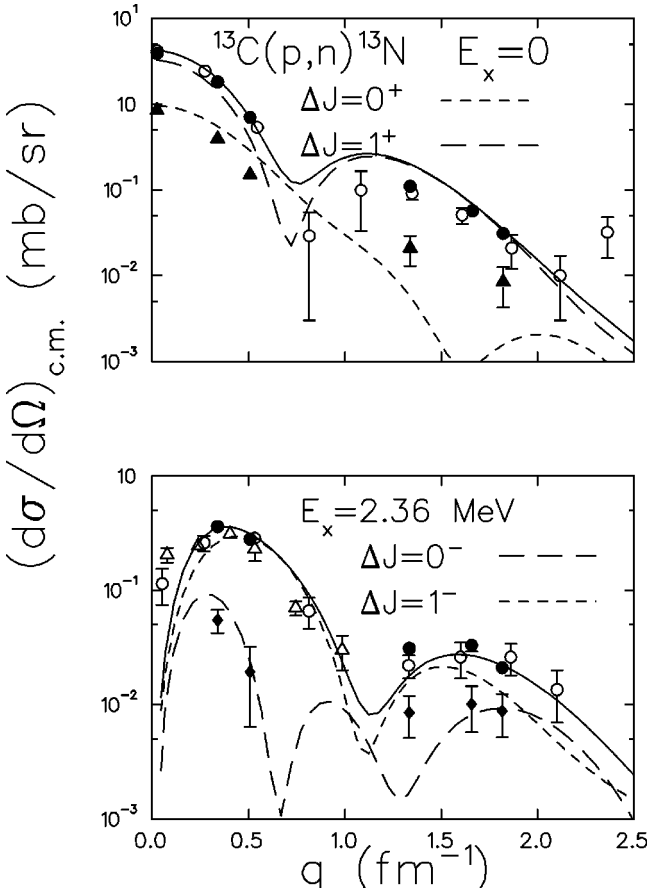

FIG. 9. Differential angular distribution cross sections for the g.s. and first excited state in the ^{13}C$(p,n)^{13}$N reaction. The solid data points correspond to this experiment. The open circle symbols and open triangle symbols correspond to data taken for these transitions at $E_p=160$ and $E_p=186$ MeV. The measured polarization-transfer coefficients have been used to deduce values for the Fermi contribution to the g.s. transition (solid triangles top frame) and to the unique spin-dipole contribution (solid diamonds bottom-frame) to the 2.36 MeV transition. The curves are DWIA calculations using the Love-Franey interaction. See text.

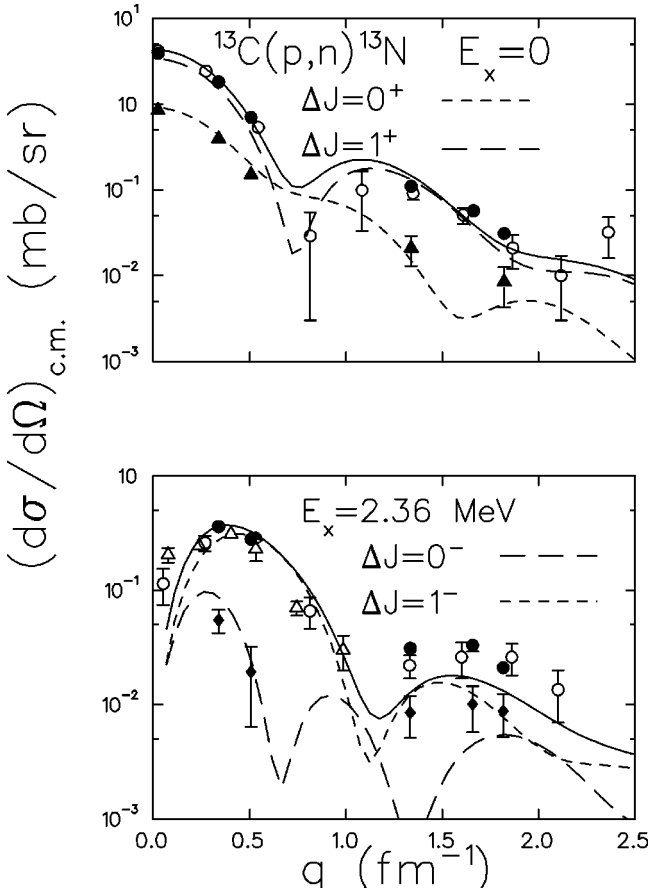

FIG. 10. Same as in Fig. 9, but curves are DWIA calculations using the DBHF interaction. See text.

observables below the pion production threshold. Details can be found in Ref. [40]. The density dependence is obtained using the DBHF approach to infinite nuclear matter. In addition to medium effects arising from Pauli blocking and correlations to the single-particle energy, this includes a proper treatment of the nucleon Dirac spinor in the medium. The G matrix thus produced is converted to a Yukawa function representation which can be used in a DWIA code. The predictions based on the DBHF interaction were obtained using DWBA86, a version of the DWIA code [27] that includes finite range DWIA for the exchange contributions. The incoming and outgoing wave distortions were calculated using a folding model potential. The nuclear charge densities for each nucleus were obtained using the parameters described in Ref. [42]. Assuming equal proton and neutron distributions, the central and spin-orbit interaction terms were averaged over the target nucleon distributions. These distributions also provided the local density at which the effective NN interaction was evaluated. In this approach, the use of a $t\rho$ approximation provides a ''self-consistent'' optical potential where the same interaction is used in the transition and in the distortion of the nucleon waves. We used the same OBDME as in the previous calculations.

Results for the angular differential cross sections calculations are presented in Fig. 10. For the g.s. transition (top frame), the GT cross section was normalized as in Fig. 9, but the Fermi contribution was normalized by a factor 2 to match the forward cross sections. There is a much better agreement with the empirical results, especially in the backward angles data, than in the previous figure. For the transition to the 2.36 MeV excited state in ^{13}N, we used a normalization of 0.28, which is the same as in the previous figure. No major improvement is noticed in this case, and it seems that the calculations shown in Fig. 9 overall show a better agreement with the data, especially in the q region between 1.3 and 2.2 fm^{-1}. The location of the zero crossing for the spin-longitudinal interaction at $q\approx 0.68$ fm^{-1} is about the same in both calculations.

There is not enough difference in the polarization-transfer coefficients calculated with the DBHF or the Love-Franey interaction to warrant additional figures. The main differences occur in the P and A_y values, but these differences are mainly in a momentum transfer region where we have no experimental data able to discriminate between the calculations.

VII. SUMMARY AND CONCLUSIONS

We have presented differential cross sections and spin-transfer coefficients for the $^{13}C(\vec{p},\vec{n})^{13}N$ reaction measured at $E_p = 197$ MeV and at angles between 0° and 33°. The data have been used to obtain natural and unnatural parity partial cross sections for transitions to the g.s. and to the first excited state (2.36 MeV) in ^{13}N. The spin-dependent cross sections have been decomposed into spin-longitudinal and spin-transverse partial cross sections. The polarization observable D_o is sizable only for the g.s. transition that includes the Fermi contribution. The other two transitions seem to be characterized by spin transfer as expected for the energy of the incident beam [1]. The empirical results for the Fermi part of the g.s. cross section are better reproduced with the DWIA calculations using the DBHF interaction. For the transition to the 2.36 MeV state in ^{13}N, the cross sections have been decomposed into spin-longitudinal ($\Delta J^\pi = 0^-$) and spin-transverse partial cross sections. The empirical data for the 0^- spin-dipole differential cross section is reproduced with either DWIA calculation but perhaps better with the Love-Franey interaction. These results are in contrast to those at 35 MeV by Orihara *et al.* [16] where it is reported that the experimental differential cross sections are much larger than IA calculations, which the authors interpreted as possible meson-exchange current effects. These data should continue to provide important tests for effective *NN* interactions as they are developed.

ACKNOWLEDGMENTS

The authors would like to acknowledge the careful work done by Bill Lozowski in preparing the targets used in these runs and also the crew of the IUCF Cyclotron. We also would like to thank J. J. Kelly for providing us the code ALLFIT. This study was supported in part by NSF Grant Nos. PHY-9722538, PHY-9803859, PHY-9409265, PHY-9602872, and PHY-0070911, and by U.S. Department of Energy Grant No. DE-FG03-00ER41148.

[1] F. Osterfeld, Rev. Mod. Phys. **64**, 491 (1992).
[2] J. Rapaport and E. Sugarbaker, Annu. Rev. Nucl. Part. Sci. **44**, 109 (1994).
[3] J. Speth and J. Wambach, in *Electric and Magnetic Giant Resonances in Nuclei*, edited by J. Speth, (World Scientific, Singapore, 1991), p. 1.
[4] S.M. Austin *et al.*, Phys. Rev. C **63**, 034322 (2001).
[5] X. Wang *et al.*, Phys. Rev. C **63**, 024608 (2001).
[6] W.M. Alberico, M. Ericson, and A. Molinari, Nucl. Phys. **A379**, 429 (1982).
[7] T. Ericson and W. Weise, *Pions and Nuclei* (Oxford University Press, New York, 1988).
[8] H. Baghaei *et al.*, Phys. Rev. Lett. **64**, 2054 (1992).
[9] F. Ajzenberg-Selove, Nucl. Phys. **A460**, 1 (1986).
[10] H. Orihara *et al.*, Phys. Rev. Lett. **49**, 1318 (1982).
[11] R. Madey *et al.*, Phys. Rev. C **56**, 3210 (1997).
[12] W.G. Love, A. Klein, M.A. Franey, and K. Nakayama, Can. J. Phys. **65**, 536 (1987).
[13] K. Hosono *et al.*, Phys. Rev. C **30**, 746 (1984).
[14] R. Sawafta *et al.*, Indiana University Cyclotron Facility Scientific and Technical Report 1988 (unpublished), p. 19.
[15] E. Stephenson (private communication).
[16] H. Orihara *et al.*, Phys. Lett. B **187**, 240 (1987).
[17] M. Palarczyk *et al.*, Nucl. Instrum. Methods Phys. Res. A **457**, 309 (2001).
[18] J.W. Watson *et al.*, in *High Energy Spin Physics*, edited by K. J. Heller and S. L. Smith, AIP Conf. Proc. No. 343 (AIP, New York, 1995), p. 203.
[19] V. Derenchuck *et al., Proceedings of the 13th International Conference on Cyclotrons and Their Applications* (World Scientific, Vancouver, Canada, 1995).
[20] S.P. Wells *et al.*, Nucl. Instrum. Methods Phys. Res. A **235**, 205 (1992).
[21] D.L. Prout *et al.*, Phys. Rev. C **65**, 034611 (2002).
[22] T.N. Taddeucci *et al.*, Phys. Rev. C **41**, 2548 (1990).
[23] L. Wang, Institute of Nuclear and Particle Physics Internal Report Ohio University INPP-93-04, 1993.
[24] J. J. Kelly, computer code ALLFIT (unpublished).
[25] X.Y. Chen *et al.*, Phys. Rev. C **47**, 2159 (1993).
[26] Y. Wang *et al.*, Phys. Rev. C **51**, 1345 (1995).
[27] R. Schaeffer and J. Raynal, computer program DWBA70, 1970 (unpublished); extended version DW81 by J. R. Comfort, 1981 (unpublished).
[28] M.A. Franey and W.G. Love, Phys. Rev. C **31**, 488 (1985).
[29] W.G. Love (private communication).
[30] B.A. Brown *et al.*, The Oxford-Buenos Aires-MSU shell model code OXBASH, Michigan State University Cyclotron Report 524, 1986.
[31] E.K. Warburton and B.A. Brown, Phys. Rev. C **46**, 923 (1992).
[32] F.P. Brady *et al.*, Phys. Rev. C **43**, 2284 (1991).
[33] R.S. Hicks *et al.*, Phys. Rev. C **26**, 339 (1982).
[34] J.R. Comfort and B.C. Karp, Phys. Rev. C **21**, 2162 (1980).
[35] P.E. Hodgson, *Nuclear Reactions and Nuclear Structure* (Clarendon, Oxford, 1971).
[36] N. Auerbach and B.A. Brown, Phys. Rev. C **65**, 024322 (2002).
[37] M, Ichimura and K. Kawahigashi, Phys. Rev. C **46**, 1822 (1992); **46**, 2117(E) (1992).
[38] E. Bleszynski, M. Bleszynski, and C.A. Whitten, Jr., Phys. Rev. C **26**, 2063 (1982).
[39] A.K. Kerman, H. McManus, and R.M. Thaler Ann. Phys. (N.Y.) **8**, 551 (1959).
[40] F. Sammarruca *et al.*, Phys. Rev. C **61**, 014309 (2000).
[41] F. Sammarruca, E.J. Stephenson, and K. Jiang, Phys. Rev. C **60**, 064610 (1999).
[42] H. de Vries, C.W. de Jager, and C. de Vries, At. Data Nucl. Data Tables **36**, 495 (1987).